Large-scale Cenozoic Wind Erosion in the Puna Plateau: The Salina del Fraile Depression

Mitchell C. McMillan[1] and Lindsay M. Schoenbohm[1,2]

[1]Department of Earth Sciences, University of Toronto, Toronto, Ontario M5S 3B1, Canada

[2] Department of Chemical and Physical Sciences, University of Toronto Mississauga, Mississauga, Ontario L5L 1C6, Canada

Corresponding author: Mitchell McMillan (mitchell.mcmillan@mail.utoronto.ca)

Key Points:

- The Salina del Fraile depression in the arid Puna Plateau was excavated by wind over the last 17 to 8.2 Ma
- Cross-sections imply up to 2 km of erosion along fold hinges, with remnant km-scale ridges and mesas analogous to landforms on Mars
- Wind can generate and sustain high relief topography, even without significant fluvial or glacial incision

Abstract

Wind erosion is integral to the evolution of arid landscapes on Earth and Mars, but the nature of long-term wind erosion of bedrock is poorly understood. Here we describe the Salina del Fraile (SdF) depression in the Puna Plateau of the Central Andes, NW Argentina, as a landform excavated by wind over several million years. New structural cross-sections and a compilation of chronostratigraphic ages rule out the hypothesis that the depression was created by transtensional tectonics. Dated remnant lacustrine and alluvial deposits in the floor of the depression constrain the rate and timing of erosion. Late Oligocene–Miocene compressional folding uplifted friable strata that were preferentially eroded, resulting in the high-relief (900 m) depression. Up to 1.95 km and an average of 1.05 km of strata were eroded during the last 8.2 to 17 Ma, at rates of 0.06 to 0.23 mm/yr. These rates are similar to long-term average wind erosion rates reported in other regions. Coarse-grained eolian megaripples, yardangs, and elongated ridges indicate ongoing eolian abrasion and deflation, aided by salt weathering, of the floor of the depression. Megaripple migration across stony lag surfaces exposes fresh bedrock to continued erosion. The SdF also contains kilometer-scale mesas and ridges that we interpret as erosional remnants. These landforms are similar to megayardangs and erosional topography identified on the lower flanks of Mount Sharp, Gale crater, Mars. In such hyperarid landscapes characterized by lithologic heterogeneities, high relief landforms can be generated and sustained by wind erosion, without significant fluvial or glacial incision.

Plain Language Summary

We investigated the origin of a large topographic depression in the arid Puna Plateau of the Central Andes, NW Argentina. Previous research interpretred the depression as formed by faulting, but we found that it is likely formed by wind erosion. While rivers and glaciers are usually responsible for high erosion on Earth, there is no evidence for river or glacier action in the Salina del Fraile. Rather, much like the surface of Mars, wind was primarily responsible for forming the depression and surrounding landscape over several million years. We show that wind was able to excavate the depression because tectonic folding brought fine-grained rocks close to the surface, where they were exposed to strong winds and breakdown by salt weathering. Wind erosion was active for the last 8.2 to 17 million years, and, as evidenced by large dust storms originating from this region, is ongoing today. Wind is lowering the surface at an average rate of 0.06 to 0.23 mm/yr, similar to previous studies. The Salina del Fraile can help researchers understand the long-term effects of wind erosion on Earth and Mars.

1 Introduction

The degree to which eolian processes shape the landscape morphology of arid regions is a long-standing point of contention (Brock & Twidale, 2011; Goudie, 2012), albeit one renewed by the exploration of wind-dominated planetary surfaces and their terrestrial analogues (e.g., Xiao et al., 2017). Recent research suggests that wind, rather than rivers or glaciers, is the dominant geomorphic agent in many parts of Earth's arid Cenozoic orogenic belts. Wind erosion may outpace fluvial incision of bedrock in hyperarid regions, and wind can enhance the erosion of favorably-oriented bedrock canyons (Perkins et al., 2015). On a regional scale, eolian deflation and abrasion can remove hundreds of meters of strata, potentially accelerating tectonic deformation (Kapp et al., 2011). Regional eolian deflation influences Earth's climate through dust emission and often results in the development of widespread desert pavements, which may drive faster surface winds through a wind-albedo-wind feedback (Pullen et al., 2018; Abell et al.,

2020). On Mars, wind-driven retreat of bedrock scarps is responsible for relatively young surface exposure ages in Gale crater, offering potential locations for sampling well-preserved complex molecules (Farley et al., 2014). Identifying regions of active eolian erosion on Mars is important for exploring geologic units that may preserve signs of ancient life (Chojnacki et al., 2018). Studying the effects of wind erosion is therefore critical for understanding how tectonic processes interact with Earth's climate, and how the surfaces of wind-dominated planets evolve over geologic time scales. Both of these efforts, however, are hampered by a relatively poor understanding of large-scale eolian landforms generated over many millions of years on Earth.

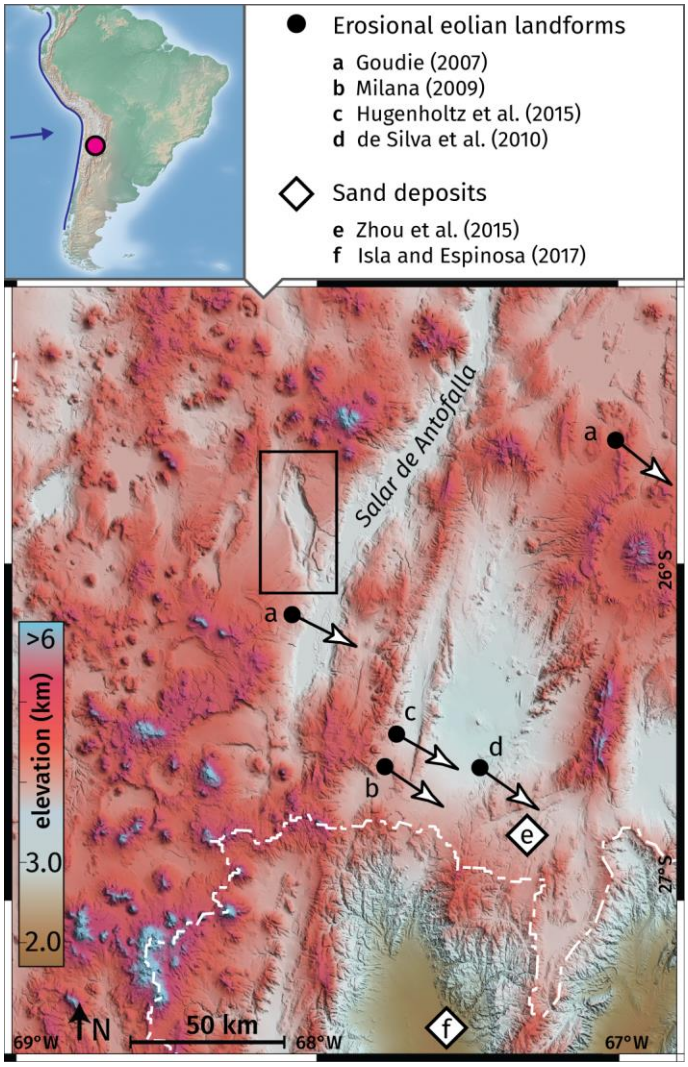

Figure 1. Digital surface model (DSM) of the southern Puna Plateau with study area boxed. Letters denote previous studies of eolian erosion (arrows) or deposition (diamonds), with arrows indicating wind direction. Inset shows study location and Nazca plate vector relative to South America. White dashed line shows limit of internally drained plateau. NASA SRTM DEM (1 arc second).

Here we show that the Salina del Fraile (SdF), a large, internally-drained depression in the southern Puna Plateau, NW Argentina, is an erosional landform excavated by wind over a time period of at least 8.2 Ma. We present new structural measurements and cross-sections that argue against tectonic lowering of the depression and instead imply up to 2 km of erosion where anticlinal folding exposed a thick package of friable, fine-grained strata. We describe remnants of alluvial surfaces within the depression to argue against significant fluvial incision during this time period. We also document eolian landforms over a wide range of spatial scales, both within and around the depression, to demonstrate the ubiquity of eolian erosion in this region. Finally, we use existing chronostratigraphic data to estimate the timing and rate of erosion and explore some implications of such long-term, large-scale wind erosion.

1.1 The Salina del Fraile

The Salina del Fraile (SdF) is an evaporite basin located to the west of the Salar de Antofalla in the southern Puna Plateau, NW Argentina (Fig. 1). Aridity in this region began as early as the Eocene (Quade et al., 2015) and intensified during the Middle to Late Miocene, when the major evaporite playas such as the Salar de Antofalla began forming (Alonso et al., 1991; Strecker et al., 2007). Regional eolian deflation commonly coincides with evaporite deposits because salt weathering disintegrates bedrock and provides fine-grained particles for removal by wind (Aref et al., 2002). Salt accumulation in closed depressions therefore tends to reinforce further eolian excavation in a positive feedback, especially if the host lithology is susceptible to salt weathering, such as would be porous sandstones or fine-grained siliciclastics (Goudie & Wells, 1995).

The SdF is situated within a continental-scale NNW–SSE eolian system, in a region characterized by erosional landforms such as yardangs, megayardangs, and periodic bedrock ridges (Fig. 1 and references therein). Significant eolian sand deposits are rare in the vicinity of the SdF, but occur further downwind in the SE Puna, in the Fiambalá basin (Fig. 1), and in a belt stretching several hundred kilometers further SE (Isla & Espinosa, 2017). Major dust storms have been imaged originating from evaporite playas on the Puna Plateau, including from the SdF (Goudie & Wells, 1995; Milana & Kröhling, 2017). Although the Puna Plateau is internally drained, sediment is removed from the southern Puna by wind, potentially providing a source of the Chaco-Pampean loess deposits in eastern Argentina (Milana & Kröhling, 2017).

The SdF-Antofalla region was tectonically deformed as it was incorporated into the Andean orogenic wedge ~30–20 Ma, uplifting and deforming a Paleogene foreland basin system (Carrapa et al., 2005; Kraemer et al., 1999; Zhou et al., 2017). Cenozoic units outcropping in the SdF consist of the Paleogene Quiñoas and Chacras Formations, a coarsening-upward sequence of continental siliciclastics; the Neogene Potrero Grande Formation, a volcaniclastic unit with interbedded ashes and ignimbrites; and later volcanic flows and ignimbrites (Kraemer et al., 1999). The Quiñoas Formation unconformably overlies Paleozoic rocks, here Permian to Jurassic sedimentary and volcanic strata exposed in the northern part of the SdF (Voss, 2002). An angular unconformity separates the Potrero Grande Formation from underlying units, which are tilted to the SE.

The SdF is a rhomboidal topographic depression, 300 km^2 in area, with up to 900 m of topographic relief. Goudie and Wells (1995) hypothesized that the SdF (therein termed Potrerillos Depression) is analogous to a giant deflation pan, “the largest Altiplano basin of primarily aeolian origin” (pg. 22), but later research in the region diverged from this

interpretation (Fig. 2). The depression's conspicuous planform shape, rectilinear slopes, and what appeared to be rotated fault blocks along the western edge (labelled "elongated ridges" in Fig. 3), led some to interpret it as a pull-apart basin, with the basin floor lowered by major normal faults as a result of a left step in an inferred N–S-trending left-lateral fault system (Reijs & McClay, 2003; Voss, 2002). Others mapped the depression as the core of an anticline with only minor faults, an interpretation that also satisfies chronostratigraphic constraints (Adelmann, 2001; Kraemer et al., 1999; Seggiaro et al., 2007). The structural interpretation of the SdF is critical, because a compressional origin requires the erosion of material in order to create a depression morphology, while a pull-apart basin would not necessitate erosion (Fig. 2).

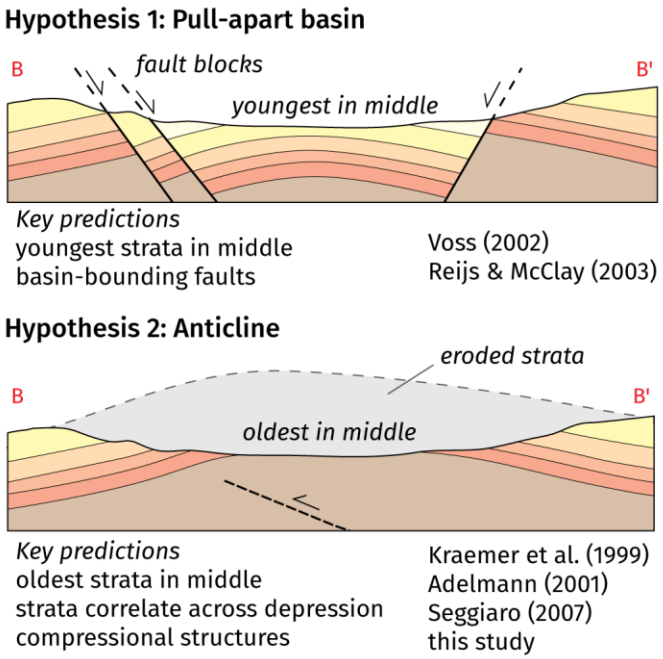

Figure 2. Theoretical cross-sections illustrating the two competing hypotheses for the origin of the Salina del Fraile depression. Strata are drawn schematically along topographic section B-B' (Fig. 3).

2 Materials and Methods

We collected measurements of bedding planes in the field using a Brunton Transit (n=40) and mapped the Cenozoic geology along two transects spanning the depression (profiles A and B in Fig. 3). Transects were oriented perpendicular to major structures, allowing us to test the two hypotheses for the formation of the depression (pull-apart basin or compressional folding). To supplement our structural data, we also digitized strikes and dips from Voss (2002, n=52) and Reijs and McClay (2003, n=39) within the Salina del Fraile by georeferencing their maps in a GIS environment. Our field measurements closely agree with nearby data from these sources. Cross-sections were constructed using the kink-band method; because a main objective is to estimate the magnitude of erosion, cross-sections were drawn to minimize the amount of eroded material, within realistic geologic constraints.

Chronostratigraphic data were compiled from Adelmann (2001, n=29), Canavan et al. (2014, n=14) and Quade et al. (2015, n=11) and mapped when sample locations were given. These data consist of single grain Ar–Ar (n=16; biotite, plagioclase, potassium feldspar), K–Ar (n=12; feldspar, biotite, glass) and U–Pb (n=21, zircon) ages and a K–Ar whole rock age (n=1, andesite). Dated lithologies were largely volcanic tuff (n=38), followed by ignimbrite (n=5), andesite (n=2) and other volcanic lithologies (n=5). The data tabulated by Adelmann (2001, Appendix 1 therein) were published in part by Kraemer et al. (1999, Table 1 therein) and the analytic methods were described by Voss (2002, Table 1 therein). Ar–Ar age determinations were performed by the GEOMAR Forschungszentrum (Kiel, Germany) and K–Ar age determinations by GEOCHRON Laboratories, Krueger Enterprises, Inc. (Cambridge, Massachusetts). U–Pb ages of volcanic zircons were published by Canavan et al. (2014, Tables DR1 and DR2 therein) and Quade et. al (2015, Table 4 therein) and were determined by laser ablation multicollector inductively coupled plasma mass spectrometry (LA-MC-ICPMS) at the University of Arizona LaserChron Center. All ages compiled here are reported with 2σ uncertainty.

For ages referenced to a stratigraphic column, we mapped the locations of the samples onto cross-section B-B' using their stratigraphic positions. Structural and chronostratigraphic data are available from McMillan and Schoenbohm (2020).

Wind directions were inferred from landforms mapped using high resolution aerial imagery provided by Bing Maps (~30 cm/px). Landforms include yardangs, megaripples, dust streaks, and abraded bedrock surfaces. We assume prevailing wind directions are well represented by the long axes of yardangs that taper downwind (n=21, Fig. 7C, e.g.); by directions normal to the average crestline orientation of asymmetric megaripples, with more gentle stoss slopes and steeper lee slopes (n=5, Fig. 8, e.g.); and by light-colored dust streaks extending downwind from evaporite or alluvial playas (n=4). Each landform yielded a single measurement of wind direction. Where fields of periodic yardangs or megaripples occur, the wind directions mapped in Fig. 3 represent an average of all measurements for the field. Although aerial imagery alone did not permit us to unambiguously distinguish the stoss and lee slopes of megaripples, their orientations and associated wind directions were verified in the field (Fig. 8A). Abraded bedrock surfaces displaying elongated ridges and grooves may also provide information about wind directions; although we are less confident about these measurements (n=2), they parallel other landforms and are therefore shown as dashed arrows in Fig. 3.

We mapped alluvial surfaces and terrace remnants in the depression using the ALOS World 3D (1 arc second) DSM provided by JAXA and verified these interpretations with field observation. The depths of internally drained portions of the landscape were analyzed using TopoToolbox (Schwanghart & Scherler, 2014).

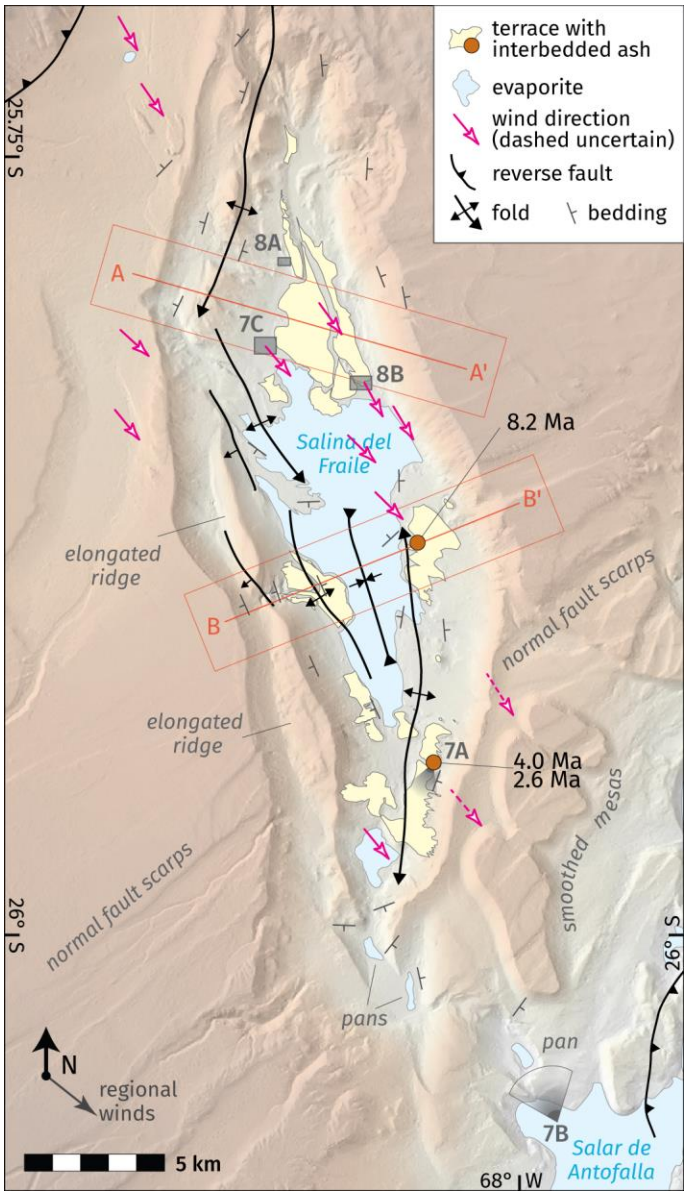

Figure 3. Topographic hillshade of the Salina del Fraile. Red boxes denote cross-sections in Fig. 4 and 5. Lettered symbols denote images in Fig. 7 and 8. Strikes and dips selected from our data, Voss (2002), and Reijs and McClay (2003). Dated ashes and their locations are from Adelmann (2001).

3 Results and Discussion

3.1 Structural interpretation: Against extensional lowering of the depression

Strata are deformed by a series of roughly N–S-trending folds, with no basin-bounding normal faults (Fig. 3). The northern portion of the SdF consists of a roughly N–S trending, southward plunging anticline that exhumes Permian and Jurassic strata (Fig. 4). The fold axis is inclined to the west, and the Potrero Grande thickens rapidly with dips decreasing up-section on

the western limb, consistent with syntectonic sedimentation (Fig. 4). On the eastern limb of the fold, late Paleogene strata are truncated by the unconformity at the base of the Potrero Grande Formation. Chronostratigraphic data confirm that the flat interior of the depression here is composed of the lower member of the Quiñoas Formation, with K–Ar ages of 37.6 of a volcanic tuff and 36.7 Ma on a reworked pumice clast (Adelmann, 2001). This interpretation is supported by U–Pb zircon ages from Canavan et al. (2014), who dated six volcanic tuffs outcropping in the eastern wall of the depression, 3.5 km north of Section A-A', with ages ranging from 36.1 Ma to 34.4 Ma.

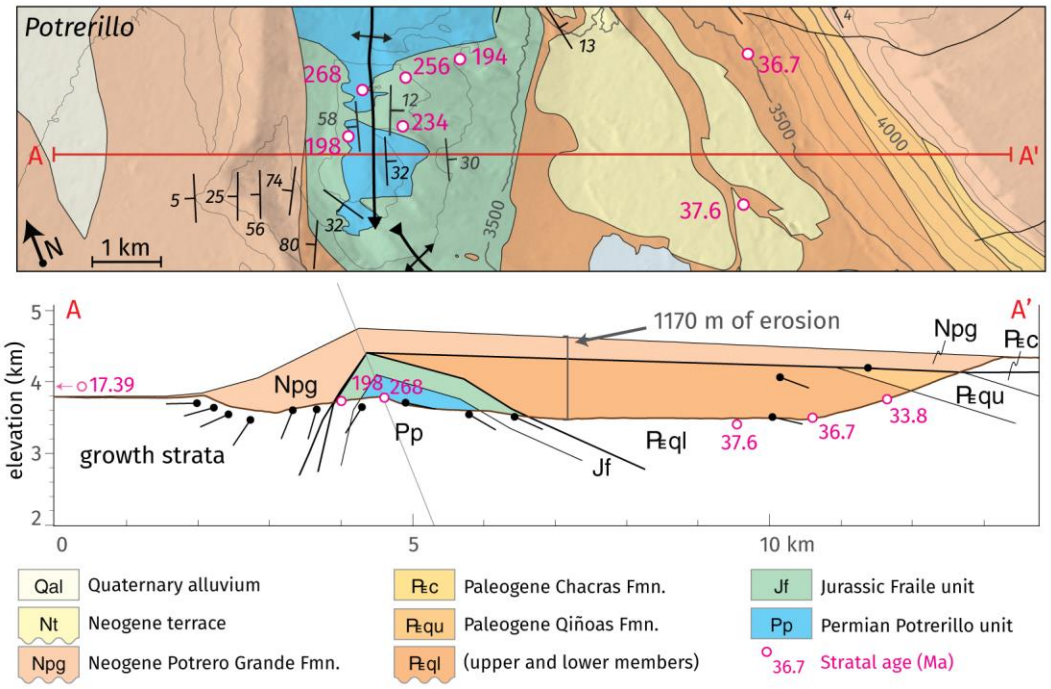

Figure 4. Section A-A'. Geologic strip-map and structural cross-section of the northern Salina del Fraile near Potrerillos. Chronostratigraphic ages compiled from Adelmann (2001), Canavan et al. (2014), and Quade et al. (2015). Strikes/dips measured in the field supplemented with those from Voss (2002) and Reijs and McClay (2003) as dark gray symbols.

The central portion of the SdF consists of a series of gentle anticlines separated by a doubly inward-plunging syncline (Fig. 5). Small kink-band folds mapped as monoclines are present on the western limb of the westernmost anticline, where strata are locally overturned. The Vega Chacras canyon on the western limb of this anticline is well-studied, with a chronostratigraphic record comprised of 17 ages in a transect across what had been interpreted as rotated fault blocks (Adelmann, 2001; Canavan et al. 2014; Quade et al., 2015). Stratal ages range from 18.0 Ma at the top of the canyon (K–Ar of volcanic glass) to 38.5 Ma near its base (U–Pb of volcanic zircon). These ages are consistent with uplifted, west-dipping, Cenozoic strata on the western limb of an anticline (Fig. 5), rather than a late Miocene normal-fault growth sequence (Reijs and McClay, 2003). We found no field evidence for repetition of strata in this

location, and stratal ages show no offsets across what had been interpreted as normal fault blocks (Fig. 5).

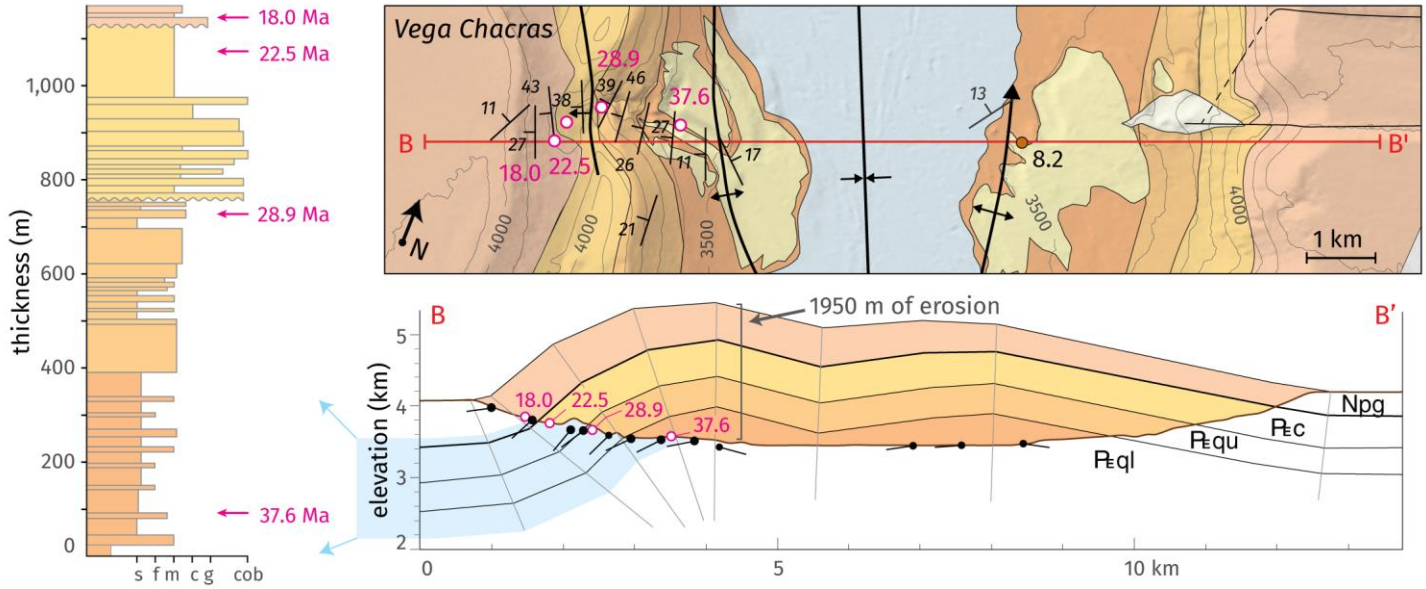

Figure 5. Section B-B'. Geologic strip-map and structural cross-section of the central Salina del Fraile near Vega Chacras. Chronostratigraphic ages selected from Adelmann (2001), Canavan et al. (2014), and Quade et al. (2015). Strikes/dips measured in the field supplemented with those from Voss (2002) and Reijs and McClay (2003) as dark gray symbols. Stratigraphic column redrawn from Adelmann (2001). Refer to Fig. 4 for legend.

The relative age of strata in the floor of the depression is a key prediction of both hypotheses (Fig. 2). Strata outcropping throughout the floor of the depression have been dated by multiple studies. Quade et al. (2015) obtained an age of 38.5 ± 0.7 Ma from an interbedded tuff near the base of Vega Chacras canyon, while Canavan et al. (2014) obtained ages of 35.7 ± 0.9 Ma and 33.9 ± 0.9 Ma from an outcrop in the southern portion of the depression. Adelmann (2001) obtained ages of 37.6 ± 0.3 Ma and 36.7 ± 0.3 Ma from bedrock exposures in the floor of the northern part of the depression. These studies indicate that the floor of the depression is composed of relatively old bedrock, the Lower Member of the Quiñoas Formation (late Eocene to early Oligocene). The lithology of this unit consists playa mudstones, evaporites, siltstones, and sandstones (Kraemer et al., 1999) up to 2 km thick in the Salina del Fraile (Fig. 4). Although the depression does contain thin Neogene terrace deposits (Fig. 4, Fig. 5, and described below), these deposits rest in angular unconformity on older units and are not consistent with structural lowering of the depression. It is possible that smaller extensional structures are hidden beneath the modern evaporite playa, but exposures of the Quiñoas would necessarily limit any such structures to a small area, and they would not be capable of explaining the origin of the depression.

These observations indicate a compressional origin for the SdF, rather than an extensional or transtensional one (Hypothesis 2, Fig. 2). The western inclination of fold axes is

consistent with fault propagation folding, possibly due to blind, west-vergent thrust faults associated with a major reverse fault system to the east (Adelmann, 2001; Voss, 2002; Seggiaro et al., 2007). The two main N-S trending anticlines in the NW and SE parts of the study area have a wavelength of ~15 km and their geometry mirrors the rhomboidal planform geometry of the depression (Fig. 3). Compressional folding and subsequent erosion thus provide a compelling explanation for the geometry of the depression.

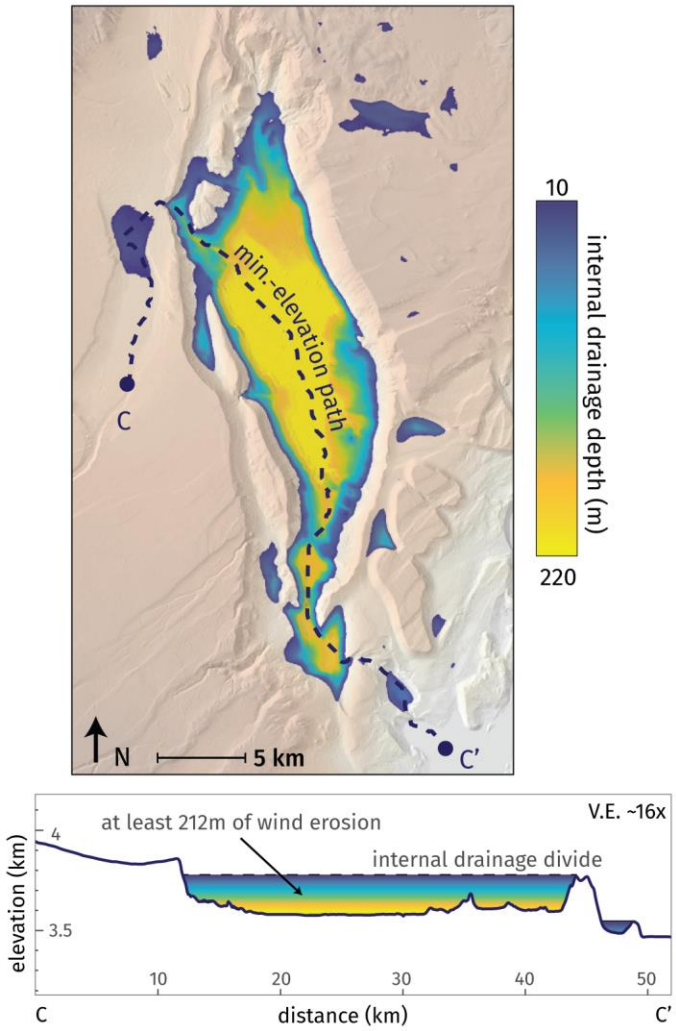

Figure 6. Internal drainage of the Salina del Fraile. The internal drainage depth approximates the minimum amount of wind (versus fluvial) erosion required to generate the observed topography. The transect follows the lowest-elevation path to the Salar de Antofalla.

3.2 Little evidence for fluvial incision

Several terraces cut into tilted Paleogene strata and capped by deposits 10–120 m thick are present within the depression (Fig. 3). The terrace deposits (lacustrine and alluvial strata with gypsum-rich soil horizons) overlie tilted Paleogene bedrock in angular unconformity (Fig. 7A)

and were deposited in an existing topographic low (Voss, 2002). The terraces have been partially eroded, and their remnants now stand in relief above the SdF floor, often as yardangs (Fig. S2B). Interbedded ashes in the terrace deposits dated to 2.6, 4.0, and 8.2 Ma (Adelmann, 2001) imply that significant erosion of the SdF occurred both before 8.2 Ma (to create the initial depression) and since 2.6 Ma (to erode the terraces and further deepen the depression). Erosional episodes were evidently punctuated by periods of net deposition or soil development.

The depression is not presently part of an integrated fluvial network. The lowest point on the southern margin of the depression is blocked by an escarpment that extends >212 m above local base level and does not appear to have been uplifted structurally (Fig. 6). Wind, which is capable of excavating internally drained depressions, is thus interpreted to be responsible for a minimum of 212 m of erosion (Fig. 6). If the depression had been externally drained when the internal Neogene terraces were deposited, they would decrease in elevation to the south (i.e., downstream); in contrast, they decrease in elevation to the north, toward the center of the depression. Terrace deposit facies are also indicative of deposition in an internally drained basin in an arid climatic regime similar to the present. Finally, late Miocene–Pliocene units ouctropping on the eastern border of the Salar de Antofalla are sourced from, and thicken toward, the Sierra de Calalaste to the east, rather than the Salina del Fraile to the west (Adelmann, 2001). It is therefore unlikely that the SdF was drained fluvially during the last 8.2 Ma (the oldest dated ash in a terrace deposit). We rule out the possibility of glacial erosion on similar grounds, with the additional point that no glacial or paleoglacial landforms are present in the Salar de Antofalla region (Haselton et al., 2002).

Structural cross-sections, drawn conservatively to minimize the amount of erosion, show that up to 1,170 m and 1,950 m of strata were removed from the northern and central SdF, respectively (Fig. 4; Fig. 5). Rather than extensional tectonics or fluvial erosion, we argue that wind is primarily responsible for forming the depression.

3.3 Evidence in favor of wind erosion

There is abundant evidence for both eolian abrasion and deflation within and around the SdF (Fig. S1; Goudie and Wells, 1995). Yardangs 10–100 m in length with ~1–5 m of relief are carved into lower Quiñoas Formation where it dips gently parallel to wind direction (Fig. 7C). Yardangs are streamlined eolian erosional landforms whose size and shape are controlled by the bedding orientation and heterogeneity of host strata (de Silva et al., 2010; Pelletier et al., 2018) as well as lithology. Five kilometers south of the yardangs, the Quiñoas Formation dips perpendicular to wind direction and outcrops as rough, sharp-crested hogbacks and smooth elongated ridges with length/width aspect ratios up to ~13 (Fig. S3C). These ridges occur over a larger area than do the yardangs and also indicate the action of eolian abrasion and deflation scouring the basin floor.

Eolian megaripples are locally present with wavelengths of 1–3 m and heights of 10–20 cm (Fig. 8; Fig. S3A). The origin of coarse-grained megaripples is debated (Milana, 2009; de Silva, 2010), but they are often thought to migrate downwind by saltation-induced creep (Lämmel, 2018). Aerial imagery reveals extensive fields of megaripples that developed on subhorizontal surfaces capped by conglomeratic deposits (Fig. 8B). The planforms of these megaripples show evidence of migration similar to that observed by Hugenholtz et al. (2015),

with orientations indicating NNW wind directions, consistent with other eolian landforms (Fig. 3). The megaripples observed in the SdF thus give additional evidence of strong winds and the presence of abrasive, saltating particles that drive their downwind migration. Their downwind migration also exposes fresh bedrock (orange surfaces visible in Fig. 8), providing a means for disrupting stony lag deposits that would otherwise protect bedrock against further erosion (Abell et al., 2020). Stony deposits are also disrupted by small gullies and rills that expose bedrock surfaces in the SE part of the depression (Fig. S2B).

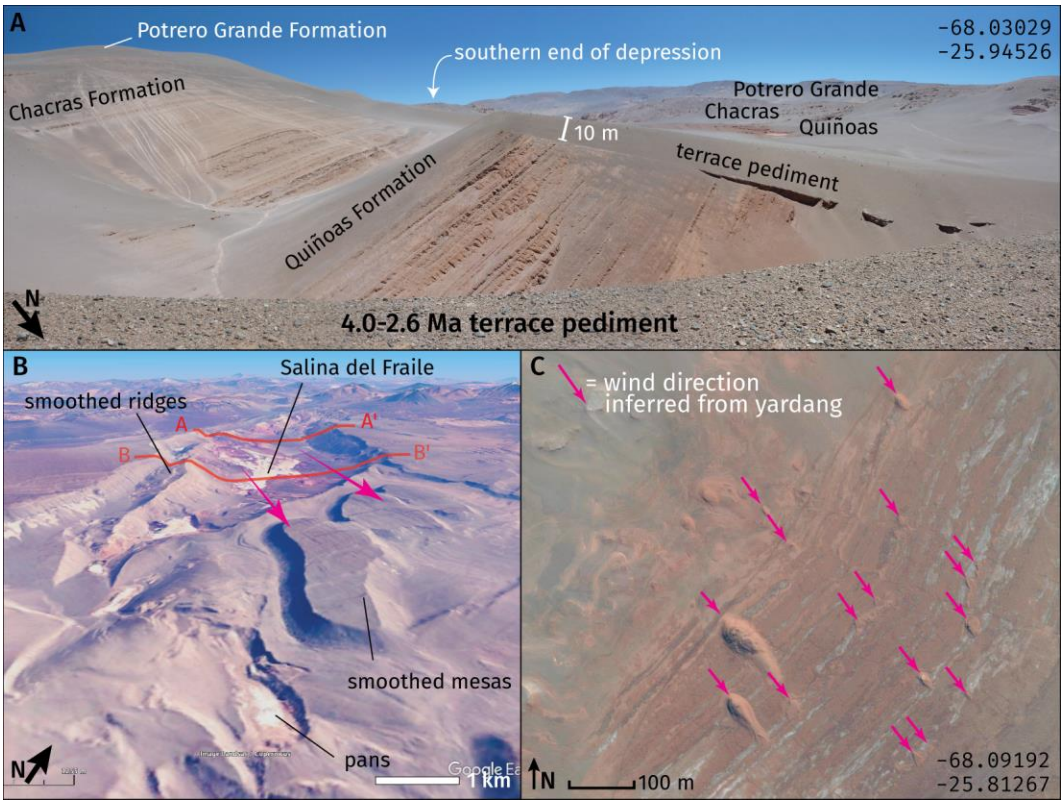

Figure 7. Geomorphological evidence of wind erosion across spatial scales. (**a**) Unconformity between 2.6–4.0 Ma terrace deposit and Cenozoic units, showing erosional streamlining of terrace edge. (**b**) Upwind view of the Salina del Fraile (Google Earth). (**c**) Yardangs carved into the friable Paleogene Quiñoas Formation. Aerial imagery from Bing Maps. Refer to Fig. 3 for the locations of images.

The sides of the depression are rectilinear bedrock slopes with nearly uniform ~27° angles (Fig. S1). The slopes have only a thin veneer of debris cover, and Cenozoic bedrock is often exposed (Fig. S3B). Alluvial rills or gullies in these slopes are rare, occurring only around localized seeps and springs. Most of these slopes have not accumulated talus at the base (Fig. S3D), while others appear to have shed a thin layer of debris into the depression (contributing the terrace deposits described above). Debris is evidently weathered and removed before it can accumulate. Because the possibility that these slopes are major fault scarps can be ruled out by our structural interpretation, these rectilinear slopes most likely retreat by weathering and eolian deflation (Selby, 1971).

Near its western rim, the SdF hosts large, smooth, elongated ridges, 5–10 km in length and up to 600 m tall (Fig. 3), elsewhere interpreted as fault scarps (Reijs and McClay, 2003). Cross section B (Fig. 5), however, indicates that these ridges are erosional. They are not parallel to wind directions inferred from smaller-scale landforms, but their long axes generally parallel the strike of underlying strata. The ridges thus reflect the strong influence of bedding orientation and lithology superimposed on erosional processes in the SdF. Their dip slopes correspond to the upper Chacras Formation, a unit of relatively resistant cross-bedded sandstones and conglomerates that contrasts with overlying Potrero Grande volcaniclastics (Adelmann, 2001). We hypothesize that these resistant strata slowed the excavation of the depression, leading to elongated erosional remnants that parallel the strike of bedding planes; these topographic remnants were likely smoothed by weathering, colluvial transport, and eolian deflation.

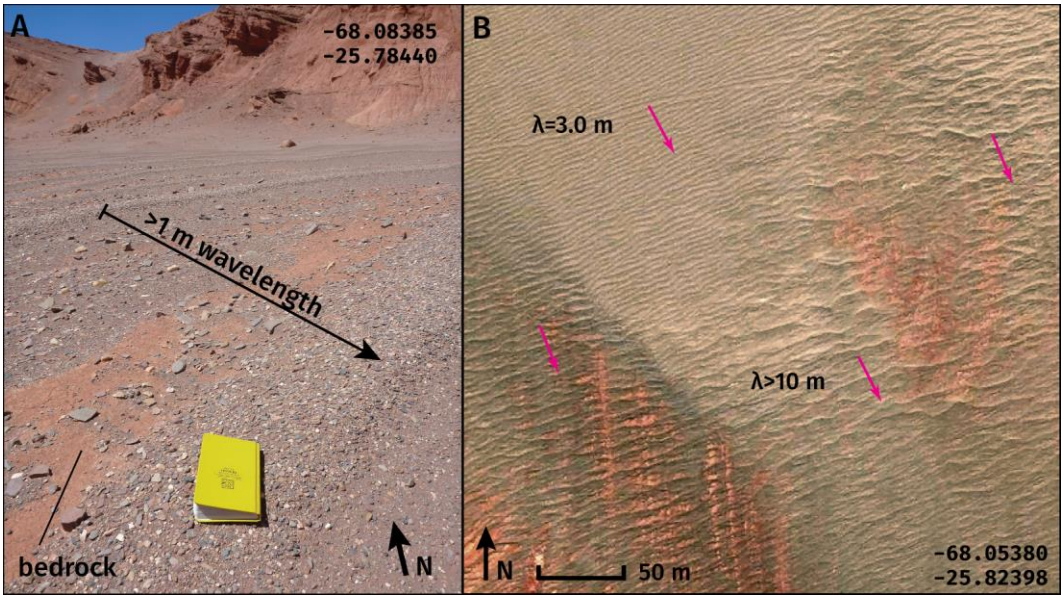

Figure 8. (**a**) Eolian megaripples photographed on a Permian bedrock surface in the Salina del Fraile. (**b**) Aerial imagery (Bing Maps) of eolian megaripples disrupting a stony lag deposit and exposing orange Quiñoas Formation bedrock. Refer to Fig. 3 for the locations of images.

Five kilometers southeast of the SdF, three ~300 m tall mesas with smooth, linear slopes are present (Fig. 3; Fig. 7B). They are 5.5–10.5 km2 in area with curvilinear planforms 2.5–6 km long that taper slightly to the SE. The tops of the mesas are subhorizontal and characterized by heavily abraded bedrock surfaces (Fig. S2D). Although the mesas resemble alluvial terraces in some respects, no evidence of fluvial channels or paleochannels is present. Instead, they correlate with a regional, subhorizontal, Late Miocene–Pliocene surface representing the top of the Potrero Grande Formation and/or Late Miocene volcanic flows in this area (Richards et al., 2006) and are therefore composed of Potrero Grande volcaniclastics.

Although it is difficult to imagine how fluvial or tectonic processes could produce these mesas, our wind erosion hypothesis provides a potential explanation. The mesas are larger and smoother than megayardangs described in indurated ignimbrites nearby on the Puna Plateau and in Northern Chile (de Silva et al., 2010), but are similar in planform shape to megayardangs in

Crommelin crater, Mars, that developed in canyon networks reworked by wind erosion (Perkins et al., 2015, and Fig. 1b therein). As evidenced by the lack of boulder-sized colluvium, the lithologic composition of the smooth mesas is weaker than well-indurated ignimbrite and not capable of supporting the near-vertical slopes characteristic of some megayardangs (de Silva et al., 2010). The volcaniclastic sediments may also be more prone to disintegration by weathering and deflation. Like terrestrial megayardangs, the smooth mesas most likely result from a combination of processes, including colluvial and alluvial diffusion, but their overall forms are indicative of eolian streamlining and deflation.

The mesas' 300 m height places them, along with a 550 m tall megayardang in the Hami basin (Pullen et al., 2018), among the tallest megayardangs known on Earth, similar in height to megayardangs of the heavily eroded Medusae Fossae Formation (MFF) on Mars, which are up to 700 m tall (Mandt et al., 2008). Unlike classic yardangs, however, the mesas are flat-topped, have low length/width aspect ratios, do not occur as a fleet of periodically spaced landforms, and their lee slopes do not gradually taper to join the surrounding topography.

The base of the smooth mesas corresponds to the contact between Potrero Grande Formation volcaniclastics and Chacras Formation conglomerates, an erodibility barrier, while the top of the mesas correlates to a regional subhorizontal surface composed of thin volcanic flows resting on top of the Potrero Grande Formation (Voss, 2002; Richards et al., 2006), which could act as a caprock. Mesa height is roughly equivalent to the thickness of the Potrero Grande Formation. The mesas are separated by abraded bedrock surfaces, mostly composed of Chacras conglomerates, with meter-scale erosional and fault scarps (Fig. S2D). These observations suggest that the mesas formed by eolian downcutting into an erodible layer underlying a resistant caprock, a model similar to one proposed for the interior of Gale crater, Mars (Day and Kocurek, 2016).

The mesas are deformed by a swarm of penetrative normal faults with 400–800 m spacing that display smaller scarps in the troughs separating the mesas than on their top surfaces (Fig. S2D). Twenty kilometers to the southwest, this fault swarm deforms volcanic flows dated to 3.61 Ma (Adelmann, 2001), indicating that a significant portion of the extensional deformation was accommodated by faulting after ~3.6 Ma. This timeframe agrees with the one we infer for wind erosion, suggesting that the smaller scarps observed in the troughs between the mesas is due to preferential erosion of the troughs during active faulting.

3.4 Timing and rate of erosion

Existing chronostratigraphic ages provide constraints on erosion rate and timing (Fig. 9). The initiation of erosion is bracketed by the top unit exposed in the depression, the Potrero Grande Formation, 17.0 Ma (Adelmann, 2001, K–Ar of biotite), and by the oldest volcanic ash deposited within the floor of the depression, 8.2 Ma (Voss, 2002, Ar–Ar of biotite). The depression must have already been partially excavated by 8.2 Ma.

Streamlining and erosion of terraces containing 2.6 Ma and 4.0 Ma ashes in the floor of the depression (Voss, 2002, Ar–Ar of plagioclase) indicates significant erosion since the Pliocene. Yardangs and megaripples, active salt weathering zones, a lack of major sedimentary fill, rectilinear bedrock slopes, and imaged dust storms all indicate that erosion is currently active in the region (Goudie and Wells, 1995; Milana and Kröhling, 2017).

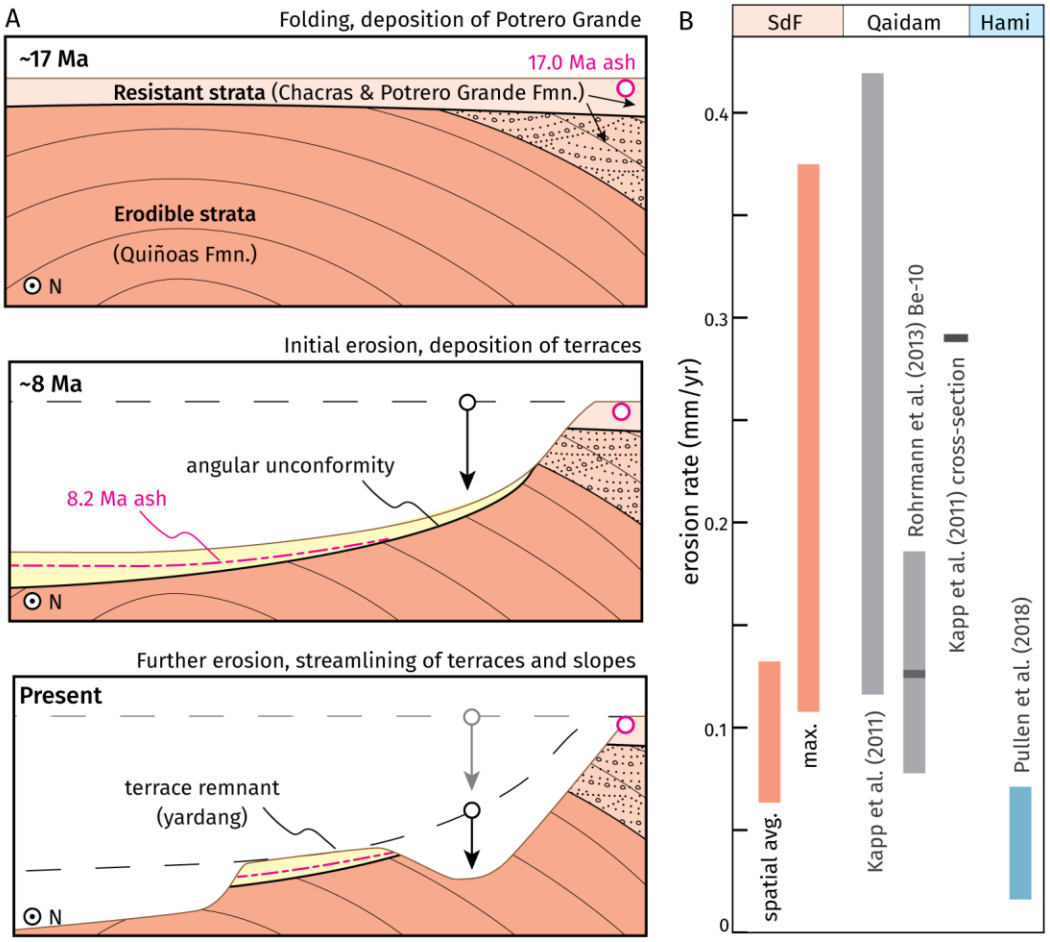

Figure 9. (**a**) Timing of wind erosion of the Salina del Fraile depression inferred from structural and chronostratigraphic data. (**b**) Comparison of erosion rates to previous long-term studies in the Qaidam Basin, China (Kapp et al., 2011; Rohrmann et al., 2013) and the Hami Basin, China (Pullen et al., 2018).

Given that erosion began between 17 and 8.2 Ma and is presently ongoing, we estimate erosion rates using the structural cross-sections presented in Section 3.1. A maximum thickness of eroded material of 1.95 km measured from section B (Fig. 5), yields maximum erosion rates of 0.11– 0.23 mm/yr in the central part of the depression. An average of 1.05 km of strata have been eroded from cross-sections A and B (Fig. 4; Fig. 5). Using this as a spatial average, wind has removed ~315 km3 of material from the depression, averaging 0.062–0.13 mm/yr. While these estimates are long-term (~107 yr), they fall within the range of long-term wind erosion rates reported elsewhere (Fig. 9B) and are 2¬–10 times lower than those calculated from cross-sections in the Qaidam basin, China, involving wind erosion of folded Pliocene strata (Kapp et al, 2011; Rohrmann et al., 2013). The spatial average erosion rate of ~0.06 mm/yr estimated here is very similar to the average erosion rate estimated for the Hami depression in northern China (Fig. 9B), which involved deflation of Neogene strata containing conglomeratic and sandstone layers (Pullen et al., 2018).

3.5 Implications

The erosional origin of the Salina del Fraile depression has implications for the late Cenozoic tectonics of the Puna Plateau. Previous researchers suggested a Pliocene phase of orogen-parallel sinistral strike-slip kinematics based on the morphology of the depression, with up to 7.7 km of offset on a purported Salina del Fraile fault system (Reijs and McClay, 2003). Such an interpretation, however, challenges measurements of nearby fault kinematics that imply orogen-parallel dextral deformation during this time (Allmendinger et al., 1989; Kraemer et al., 1999; Zhou et al., 2015). Our inference that the depression is erosional obviates the need to invoke orogen-parallel sinistral tectonics and implies that Pliocene to Recent extensional deformation was accommodated by the normal faults apparent in Figure 3, which may be splays off the dextral Acazoque fault system that terminates near the Salar de Antofalla (Kraemer et al., 1999).

The initiation of wind erosion between 17 and 8.2 Ma is broadly consistent with a documented phase of aridification on the Puna Plateau partially driven by the uplift of ranges east of the study area (Strecker et al., 2007), such as the Sierra Laguna Blanca (exhumed 15–10 Ma; Zhou et al., 2017). Late Miocene aridification is also partially attributed to global cooling forced by a decline in atmospheric CO2 (Herbert et al., 2016). Global aridification and cooling during the Late Miocene is reflected in ocean temperature proxies and in various moisture and temperature proxies compiled throughout Eurasia (Miao et al., 2012). Large-scale eolian deflation and excavation of topographic depressions, such as the Salina del Fraile and the Hami basin in central Asia (Pullen et al., 2018) may represent a topographic signal of this episode of global climate change. Alternatively, existing data also permit the interpretation that erosion began as soon as the package of friable strata was tectonically deformed and exposed ~17 Ma.

The idea that high-relief topography can be generated and sustained by eolian processes, with magnitudes of deflation up to 2 km, has implications for similar landforms on Earth and other planetary surfaces. The Central Andes hosts several depressions 10–50 km in width that, while little studied, may have been partially formed by wind erosion (Fig. 1). Previous research indicates that the Purulla Basin (Fig. 1, location B) may have experienced an average deflation of roughly ~4 m during the Holocene, approximately 0.3 mm/yr (Milana and Kröhling, 2017). Although more work should be done to quantify erosion rates in wind-dominated areas of the Puna, the Salina del Fraile suggests that the magnitude of eolian erosion throughout the Cenozoic may be significant in these internally drained regions lacking major fluvial incision.

Many martian landforms are thought to be formed by wind erosion over long timescales. Mounds of sedimentary strata located in the centers of impact craters preserve records of past

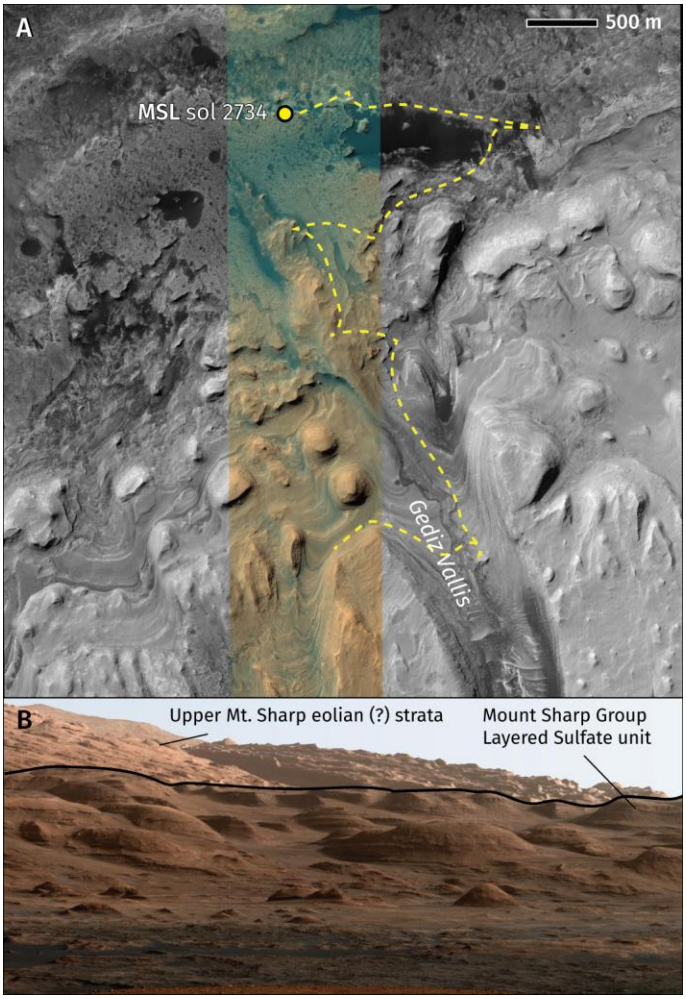

climates and are important exploration targets (Anderson and Bell, 2010). A substantial amount of wind erosion (up to a few km) is necessary to form the present morphology of many central mounds, whether they are remnants of crater-filling material (Bennett and Bell, 2016; Steele et al., 2018), or they formed in-place (Kite et al., 2013). The lower flank of Mount Sharp, the central mound of Gale crater, consists of erosional buttes, mesas, and canyons that strongly resemble the smoothed mesas and elongated ridges described above (Fig. 10).

Figure 10. Eolian landforms in Gale crater, Mars, analogous to the smooth mesas near Salina del Fraile, Argentina. (**a**) Strata on the the NW flank of Mt. Sharp are eroded into streamlined mesas and buttes of the Layered Sulfate unit of the Mount Sharp Group (stratigraphy of Fraeman et al., 2016). Yellow line approximates the proposed path of the Mars Science Laboratory Curiosity rover (MSL). Cutout from MRO/HiRISE image ESP_061961_1750_MIRB (NASA/JPL/University of Arizona). (**b**) Portion of white-balanced photomosaic of lower Mt. Sharp showing the profile of these streamlined erosional buttes and mesas. Acquired by

Curiosity's Mast Camera (Mastcam) on September 20, 2012 (PIA16768; NASA/JPL-Caltech/MSSS).

Mudstones on the floor of Gale crater have exposure ages of only 78 ± 30 Ma, likely due to wind-driven bedrock scarp retreat (Farley et al., 2014). This relatively recent exposure increases the likelihood that complex organic molecules are preserved in near-surface materials. Identifying regions of rapid wind erosion is therefore critical for future missions exploring potentially habitable environments on Mars (Chojnacki et al., 2018). Like Gale and other martian craters including Jezero, the proposed landing site of the Perseverance rover, portions of the interior of the SdF are characterized by ongoing eolian erosion of lacustrine and alluvial strata that once partially filled the depression (Palucis et al., 2016; Chojnacki et al., 2018). The SdF thus represents a terrestrial analogue to martian landforms that are the target of exploratory missions.

5 Conclusions

Structural and chronostratigraphic data show that the SdF depression was excavated by erosion of up to 2 km of friable, Paleogene strata exposed in compressional folds. Wind, rather than water or ice, was the dominant agent of erosion during at least the past 8.2 Ma. This inference is based on depositional ages of alluvial and lacustrine deposits contained within the depression, the prevalence of erosional eolian landforms within and around the depression, the lack of integrated fluvial networks, and the regional geomorphic context, which is presently dominated by wind erosion.

Inferred erosion rates are of 0.06–0.23 mm/yr are typical of arid regions on Earth, but the large magnitude of erosion reflects the long time period (>8.2 Ma) during which eolian deflation took place. The SdF documents a long-term source of eolian sand and dust in the southern Puna Plateau, and exhibits some of the largest eolian landforms on Earth. In addition to the SdF depression itself, these include kilometer-scale elongated ridges and smoothed mesas resembling megayardangs and eolian landforms on Mars. Due to lithologic variation and tectonic folding, which produce erodibility contrasts, these high-relief landforms can be sustained without significant fluvial or glacial incision. Although the SdF is particularly well-studied, similar internally drained depressions in the Central Andes and other regions may have been partially formed by wind erosion. Study of these landforms may yield insights into the evolution of Earth's arid regions on timescales of 10^6–10^7 yr, including how tectonic deformation and climate interact in such landscapes

Acknowledgments

The authors have no conflicts of interest to disclose. Support for this work was provided by an NSERC Discovery Grant and Discovery Accelerator Supplement to L. Schoenbohm. We thank Yanina Rojo and Santiago Uriburu Q. for assistance in the field, and we are grateful to Erin Seagren and Jeremy Rimando for helpful advice and discussions that strengthened the manuscript. Structural and geochronological data for this research are available in McMillan and Schoenbohm (2020) and online at https://doi.org/10.5683/SP2/UHDHGY.

References

Abell, J. T., Pullen, A., Lebo, Z. J., Kapp, P., Gloege, L., Metcalf, A. R., Nie, J., & Winckler, G. (2020). A wind-albedo-wind feedback driven by landscape evolution. *Nature Communications, 11,* 1–9. https://doi.org/10.1038/s41467-019-13661-w

Adelmann, D. (2001). Känozoische Beckenentwicklung des zentralandinen Puna-Plateaus (NW-Argentinien): Das Gebiet um den Salar de Antofalla und ein Vergleich zur nördlichen Puna, (Doctoral dissertation). Berlin: Freien Universität Berlin.

Allmendinger, R. W., Strecker, M., Eremchuk, J. E., & Francis, P. (1989). Neotectonic deformation of the southern Puna Plateau, northwestern Argentina. *Journal of South American Earth Sciences, 2,* 111–130. https://doi.org/10.1016/0895-9811(89)90040-0

Alonso, R. N., Jordan, T. E., Tabbutt, K. T. and Vandervoort, D. S. (1991). Giant evaporite belts of the Neogene central Andes. *Geology, 19,* 401–404.

Anderson. R. B., & Bell, J. F. III. (2010). Geologic mapping and characterization of Gale Crater and implications for its potential as a Mars Science Laboratory landing site. *Mars, 5,* 76–128. https://doi.org/10.1555/mars.2010.0004

Aref, M. A. M., El-Khoriby, E., & Hamdan, M. A. (2002). The role of salt weathering in the origin of the Qattara Depression, Western Desert, Egypt. *Geomorphology*, *45*(3-4), 181–195. https://doi.org/10.1016/S0169-555X(01)00152-0

Bennett, K. A., & Bell, J. F. III. (2016). A global survey of martian central mounds: Central mounds as remnants of previously more extensive large-scale sedimentary deposits. *Icarus, 264,* 331–341. https://doi.org/10.1016/j.icarus.2015.09.041

Brock, E. J. and Twidale, C. R. (2011). J. T. Jutson and the work of the wind in shaping the landscape. *Geographical Research, 49,* 47–58. https://doi.org/10.1111/j.1745-5871.2010.00662.x

Canavan, R. R., Carrapa, B., Clementz, M. T., Quade, J., DeCelles, P. G., & Schoenbohm, L. M. (2014). Early Cenozoic uplift of the Puna plateau, Central Andes, based on stable isotope paleoaltimetry of hydrated volcanic glass. *Geology, 42,* 447–450. https://doi.org/10.1130/G35239.1

Carrapa, B., Adelmann, D., Hilley, G. E., Mortimer, E., Sobel, E. R., & Strecker, M. R. (2005). Oligocene range uplift and development of plateau morphology in the southern central Andes. *Tectonics, 24,* TC4011. https://doi.org/10.1029/2004TC001762

Chojnacki, M., Banks, M., & Urso, A. (2018). Wind-driven erosion and exposure potential at Mars 2020 rover candidate-landing sites. *Journal of Geophysical Research: Planets, 123,* 468–488. https://doi.org/10.1002/2017JE005460

Day, M., & Kocurek, G. (2016). Observations of an aeolian landscape: From surface to orbit in Gale Crater. *Icarus, 280,* 37–71. https://doi.org/10.1016/j.icarus.2015.09.042

DeCelles, P. G., Carrapa, B., Horton, B. K., McNabb, J., Gehrels, G. E., & Boyd, J. (2015). The Miocene Arizaro Basin, central Andean hinterland: Response to partial lithosphere removal? *Geological Society of America Memoirs, 212,* 359–386. https://doi.org/10.1130/2015.1212(18)

de Silva, S. L., Bailey, J. E., Mandt, K. E., & Viramonte, J. M. (2010). Yardangs in terrestrial ignimbrites: Synergistic remote and field observations on Earth with applications to Mars. *Planetary and Space Science, 58,* 459–471. https://doi.org/10.1016/j.pss.2009.10.002

de Silva, S. L. (2010). The largest wind ripples on Earth: COMMENT. *Geology, 38,* e218. https://doi.org/10.1130/G30780C.1

Farley, K. A. et al. (2014). In situ radiometric and exposure age dating of the Martian surface. *Science, 343,* 1247166. https://doi.org/10.1126/science.1247166

Fraeman, A. A., Ehlmann, B. L., Arvidson, R. E., Edwards, C. S., Grotzinger, J. P., Milliken, R. E., Quinn, D. P., & Rice, M. S. (2016). The stratigraphy and evolution of lower Mount Sharp from spectral, morphological, & thermophysical orbital data sets. *Journal of Geophysical Research: Planets, 121,* 1713–1736. https://doi.org/10.1002/2016JE005095

Goudie, A. S. (2007). Mega-yardangs: A global analysis. *Geography Compass, 1,* 65–81. https://doi.org/10.1111/j.1749-8198.2006.00003.x

Goudie, A. S. (2012). Charles Rollin Keyes and extravagant aeolation. *Aeolian Research, 4,* 51–53. https://doi.org/10.1016/j.aeolia.2012.01

Goudie, A. S., & Wells, G. L. (1995). The nature, distribution and formation of pans in arid zones. *Earth Science Reviews, 38,* 1–69. https://doi.org/10.1016/0012-8252(94)00066-6

Haselton, K., Hilley, G., & Strecker, M. R. (2002). Average Pleistocene climatic patterns in the southern central Andes: Controls on mountain glaciation and paleoclimate implications. *Journal of Geology, 110,* 211–226. https://doi.org/10.1086/338414

Herbert, T. D., Lawrence, K. T., Tzanova, A., Peterson, L. C., Caballero-Gill, R., & Kelly, C. S. (2016). Late Miocene global cooling and the rise of modern ecosystems. *Nature Geoscience, 9,* 843–847. https://doi.org/10.1038/ngeo2813

Hermanns, R. L., Niedermann, S., Villanueva Garcia, A., Gomez, J. S., & Strecker, M. R. (2001). Neotectonics and catastrophic failure of mountain fronts in the southern intra-Andean Puna Plateau, Argentina. *Geology, 29,* 619–623. https://doi.org/10.1130/0091-7613(2001)029<0619:NACFOM>2.0.CO;2

Hugenholtz, C. H., Barchyn, T. E., & Favaro, E. A. (2015). Formation of periodic bedrock ridges on Earth. *Aeolian Research, 18,* 135–144. https://doi.org/10.1016/j.aeolia.2015.07.002

Isla, F. and Espinosa, M. (2017). Upper Quaternary evolution of the dune field of the Bolsón de Fiambalá, Catamarca: Sand dispersal at the Andes piedmonts. *Quaternary International, 442,* 59–66. https://doi.org/10.1016/j.quaint.2016.07.037

Kapp, P., Pelletier, J. D., Rohrmann, A., Heermance, R., Russell, J., & Ding, L. (2011). Wind erosion in the Qaidam basin, central Asia: Implications for tectonics, paleoclimate, and the source of the Loess Plateau. *GSA Today, 21,* 4–10. https://doi.org/10.1130/GSATG99A.1

Kite, E. S., Lewis, K. W., Lamb, M. P., Newman, C. E., & Richardson, M. I. (2013). Growth and form of the mound in Gale Crater, Mars: Slope wind enhanced erosion and transport. *Geology, 41,* 543–546. https://doi.org/10.1130/G33909.1

583 Kraemer, B., Adelmann, D., Alten, M., Schnurr, W., Erpenstein, K., Kiefer, E., van den Bogaard,
584 P., & Görler, K. (1999). Incorporation of the Paleogene foreland into the Neogene Puna
585 plateau: The Salar de Antofalla area, NW Argentina. *Journal of South American Earth*
586 *Sciences, 12*, 157–182. https://doi.org/10.1016/S0895-9811(99)00012-7

587 Lämmel, M., Meiwald, A., Yizhaq, H., Tsoar, H., Katra, I., & Kroy, K. (2018). Aeolian sand
588 sorting and megaripple formation. *Nature Physics, 14*, 759–765.
589 https://doi.org/10.1038/s41567-018-0106-z

590 Mandt, K. E., de Silva, S. L., Zimbelman, J. R., & Crown, D. A. (2008). Origin of the Medusae
591 Fossae Formation, Mars: Insights from a synoptic approach. *Journal of Geophysical*
592 *Research: Planets, 113*, E12011. https://doi.org/10.1029/2008JE003076

593 McMillan, M & Schoenbohm, L. M. (2020). Large-Scale Cenozoic Wind Erosion in the Puna
594 Plateau, *Scholars Portal Dataverse*, V1, UNF:6:IYumHRpsKMuN/fEcJ4fjWQ==
595 [fileUNF]. https://doi.org/10.5683/SP2/UHDHGY

596 Miao, Y., Herrmann, M., Wu, F., Yan, X., & Yang, S. (2012). What controlled Mid-Late
597 Miocene long-term aridification in Central Asia? - Global cooling or Tibetan Plateau
598 uplift: A review. *Earth-Science Reviews, 112*, 155–172,
599 https://doi.org/10.1016/j.earscirev.2012.02.003

600 Milana, J. P. (2009). Largest wind ripples on Earth?. *Geology, 37*, 343–346.
601 https://doi.org/10.1130/G25382A.1

602 Milana, J. P. and Kröhling, D. M. (2017). First data on volume and type of deflated sediment
603 from Southern Puna Plateau and its role as source of the Chaco-Pampean loess.
604 *Quaternary International, 438*, 126–140. https://doi.org/10.1016/j.quaint.2017.03.007

605 Palucis, M. C., Dietrich, W. E., Williams, R. M. E., Hayes, A. G., Parker, T., Sumner, D. Y.,
606 Mangold, N., Lewis, K., & Newsom, H. (2016). Sequence and relative timing of large
607 lakes in Gale crater (Mars) after the formation of Mount Sharp. *Journal of Geophysical*
608 *Research: Planets, 121*, 472–496. https://doi.org/10.1002/2015JE004905

609 Pelletier, J. D., Kapp, P. A., Abell, J., Field, J. P., Williams, Z. C., & Dorsey, R. J. (2018).
610 Controls on yardang development and morphology: 1. Field observations and
611 measurements at Ocotillo Wells, California. *Journal of Geophysical Research*: *Earth*
612 *Surface, 123*, 694–722. https://doi.org/10.1002/2017JF004461

613 Perkins, J. P., Finnegan, N. J., & de Silva, S. L. (2015). Amplification of bedrock canyon
614 incision by wind. *Nature Geoscience, 8*, 305–310. https://doi.org/10.1038/ngeo2381

615 Pullen, A., Kapp, P., & Chen, N. (2018). Development of stratigraphically controlled, eolian-
616 modified unconsolidated gravel surfaces and yardang fields in the wind-eroded Hami
617 Basin, northwestern China, Geological Society of America Bulletin, *130*, 630–648.
618 https://doi.org/10.1130/B31734.1

619 Quade, J., Dettinger, M. P., Carrapa, B., DeCelles, P. G., Murray, K. E., Huntington, K. W.,
620 Cartwright, A., Canavan, R. R., Gehrels, G., & Clementz, M. (2015). The growth of the
621 central Andes, 22° S-26° S., in DeCelles, P. G., Ducea, M. N., Carrapa, B., & Kapp, P.
622 A., eds., Geodynamics of a Cordilleran Orogenic System: The Central Andes of
623 Argentina and Northern Chile. *Geological Society of America Memoir 212*, 277–308.
624 https://doi.org/10.1130/2015.1212(15)

Reijs, J., & McClay, K. (2003). The Salina del Fraile pull-apart basin, northwest Argentina. In Storti, F., Holdsworth, R. E., & Salvini, F. (Eds.), *Intraplate Strike-Slip Deformation Belts, Special Publication Series* (Vol. 210, pp. 197–209). London: The Geological Society of London. https://doi.org/10.1144/Gsl.Sp.2003.210.01.12

Richards, J. P., Ullrich, T., & Kerrich, R. (2006). The Late Miocene-Quaternary Antofalla volcanic complex, southern Puna, NW Argentina: Protracted history, diverse petrology, and economic potential. *Journal of Volcanology and Geothermal Research, 152,* 197–239. https://doi.org/10.1016/j.jvolgeores.2005.10.006

Rohrmann, A., Heermance, R., Kapp, P., & Cai, F. (2013). Wind as the primary driver of erosion in the Qaidam Basin, China. *Earth and Planetary Science Letters, 374,* 1–10. https://doi.org/10.1016/j.epsl.2013.03.011

Schwanghart, W., & Scherler, D. (2014). TopoToolbox 2 – MATLAB-based software for topographic analysis and modeling in Earth surface sciences. *Earth Surface Dynamics, 2,* 1–7. https://doi.org/10.5194/esurf-2-1-2014

Seggiaro, R., Becchio, R., Pereyra, F., & Martínez, L. (2007). *Hoja Geológica 2569-IV, Antofalla, provincias de Catamarca y Salta* (Boletín 343, scale 1:250,000). Buenos Aires: Instituto de Geología y Recursos Minerales, Servicio Geológico Minero Argentina, Programa Nacional de Cartas Geológicas. https://repositorio.segemar.gob.ar/handle/308849217/97

Selby, M. J. (1971). Slopes and their development in an ice-free, arid area of Antarctica: *Geografiska Annaler: Series A, Physical Geography, 53,* 235–245. https://doi.org/10.1080/04353676.1971.11879849

Steele, L. J., Kite, E. S., & Michaels, T. I. (2018). Crater mound formation by wind erosion on Mars. *Journal of Geophysical Research: Planets, 123,* 113–130. https://doi.org/10.1002/2017JE005459

Strecker, M. R., Alonso, R. N., Bookhagen, B., Carrapa, B., Hilley, G. E., Sobel, E. R., & Trauth, M. H. (2007). Tectonics and climate of the southern Central Andes. *Annual Review of Earth and Planetary Sciences, 35,* 747–787. https://doi.org/10.1146/annurev.earth.35.031306.140158

Voss, R. (2002). Cenozoic stratigraphy of the southern Salar de Antofalla region, northwestern Argentina. *Andean Geology, 29,* 167–189. https://doi.org/10.4067/S0716-02082002000200002

Xiao, L., Wang, J., Dang, Y., Cheng, Z., Huang, T.,Zhao, J., Xu, Y., Huang, J., Xiao, Z., & Komatsu, G. (2017). A new terrestrial analogue site for Mars research: The Qaidam Basin, Tibetan Plateau (NW China). *Earth-Science Reviews, 164,* 84–101. https://doi.org/10.1016/j.earscirev.2016.11.003

Zhou, R., Schoenbohm, L. M., & Cosca, M. (2015). Recent, slow normal and strike-slip faulting in the Pasto Ventura region of the southern Puna Plateau, NW Argentina. *Tectonics, 32,* 19–33. https://doi.org/10.1029/2012TC003189

Zhou, R., Schoenbohm, L. M., Sobel, E. R., Davis, D. W., & Glodny, J. (2017). New constraints on orogenic models of the southern Central Andean Plateau: Cenozoic basin evolution

and bedrock exhumation. *Geological Society of America Bulletin*, *129*, 152–170. https://doi.org/10.1130/B31384.1